ADVANCED FUNCTIONAL MATERIALS
www.afm-journal.de

A Dual-Layered Microfluidic System for Long-Term Controlled In Situ Delivery of Multiple Anti-Inflammatory Factors for Chronic Neural Applications

Laura Frey, Praveen Bandaru, Yu Shrike Zhang, Kevin O'Kelly, Ali Khademhosseini,* and Su Ryon Shin**

This study reports the development of a microfluidic system capable of repeated infusions of anti-inflammatory factors post-implantation for use as a coating for neural probes. This system consists of a microchannel in a thin gelatin methacryloyl–polyethylene glycol composite hydrogel surrounded by a porous polydimethylsiloxane membrane, where the hydrogel can be dried to increase the stiffness for easy insertion. Reswelling allows the perfusion of interleukin (IL)-4 and dexamethasone as anti-inflammatory factors through the channel with minimal burst release and significant amounts of IL-4 are observed to release for up to 96 h post-infusion. Repeated injections of IL-4 increase the ratio of prohealing M2 versus proinflammatory M1 phenotypes of macrophages encapsulated in the hydrogel by sixfold compared with a single injection, over a 2-week period. These repeated infusions also significantly downregulate the expression of inflammatory markers tumor necrosis factor-α and IL-6 in astrocytes encapsulated in hydrogel. To demonstrate the system as a coating of neural probes for in vivo applications, a prototype device is further fabricated, where a thin dual-layered microfluidic system is integrated onto a metal probe. Such a drug delivery system can help reduce the formation of a glial scar around neural probes.

1. Introduction

In recent years, considerable advances have been made regarding the use of neural electrodes to not only measure and record brain functionality, but to suppress or stimulate different areas of the brain in order to treat a variety of conditions.[1] These electrodes have been successfully employed to minimize the effects of motor neuronal disease,[2] Parkinson's disease,[3] epilepsy,[3a,b,4] and to overcome the effects of paralysis.[1b,5] Furthermore, advancements are being made in the use of electrodes to combat deafness and blindness through cochlear and retinal implants and to reduce the effects of mood disorders by deep brain stimulation (DBS).[3,4]

The short-term successes of these implants are well-documented with DBS now being a U.S. Food and Drug Administration-approved treatment for dystonia, Parkinson's, and essential tremor in the US.[1c] However, there have been challenges with long-term utilization of these electrodes. Sometimes positive initial results and reductions in symptoms reduce over time as the electrodes become less effective.[1b,6] This reduction in effectiveness is usually attributed to the gradual encapsulation of the electrode by scar tissues and therefore the issue cannot be dealt with by simply replacing an electrode. This can be attributed to the initial insertion-associated injury (acute response),[7] presence of a foreign material (chronic response),[2,15] damage caused by micromotion of the inserted electrode,[1a,3c,8] or repeated electrical overstimulation of the tissue.[9] For these reasons, much of the research has focused on making the electrodes as small and biocompatible as possible, with recent

Dr. L. Frey, P. Bandaru, Dr. Y. S. Zhang, Prof. A. Khademhosseini, Dr. S. R. Shin
Biomaterials Innovation Research Center
Division of Engineering in Medicine
Department of Medicine
Brigham and Women's Hospital
Harvard Medical School
Cambridge, MA 02139, USA
E-mail: alik@bwh.harvard.edu; sshin4@partners.org

Dr. L. Frey, P. Bandaru, Dr. Y. S. Zhang, Prof. A. Khademhosseini, Dr. S. R. Shin
Harvard-MIT Division of Health Sciences and Technology
Massachusetts Institute of Technology
Cambridge, MA 02139, USA

The ORCID identification number(s) for the author(s) of this article can be found under https://doi.org/10.1002/adfm.201702009.

DOI: 10.1002/adfm.201702009

Dr. L. Frey, Prof. K. O'Kelly
Trinity Centre of Bioengineering
Trinity College Dublin
Dublin 2, Ireland
E-mail: okellyk@tcd.ie

Dr. Y. S. Zhang, Prof. A. Khademhosseini, Dr. S. R. Shin
Wyss Institute for Biologically Inspired Engineering
Harvard University
Boston, MA 02115, USA

Prof. A. Khademhosseini
Department of Bioindustrial Technologies
College of Animal Bioscience and Technology
Konkuk University
Hwayang-dong, Kwangjin-gu, Seoul 143-701, Republic of Korea

Prof. A. Khademhosseini
Nanotechnology Center
King Abdulaziz University
Jeddah 21569, Saudi Arabia

research also highlighting the importance of matching biomechanical properties.

Several recent studies have shown that strategies that effectively reduce the acute anti-inflammatory response to implants often are indistinguishable from untreated devices at the chronic stage of implantation. For example, a study by Potter et al.[10] where neural implants released curcumin from polyvinyl alcohol film coatings over time, with most of the release occurring in the first 10 h, showed a reduction in scar tissue and an increase in functioning neurons surrounding the implant at 4 weeks. However, once a time of 12 weeks was reached, there was no statistical difference between the implants that were drug-eluting and those that were not. Although not a drug-eluting probe, the same phenomenon was found when investigating the shape and size effects on glial scarring in a study by Szarowski et al.[8a] Smaller rounded implants showed a reduction in the acute response of microglia (defined as less than 2 weeks in this study) but chronic results from 4 weeks to up to 12 weeks showed no significant difference between all designs.[8a]

These studies indicate that, in order to create viable probes for long-term implantation, a strategy to reduce the inflammatory reaction of the brain tissue in its chronic phase is required. The definition of chronic itself is up for debate, with many studies not defining what they deem to be chronic at all, or suggestions ranging from 1 to 12 weeks with most settling around the 2–4 week mark.[11] For this study, a chronic phase is considered as 2 weeks or greater as this has been indicated to be the transition point.[12] This study thus considered the design and optimization of a dual-layered microfluidic system that would allow for long-term and steady delivery of an optimized profile of anti-inflammatory drugs and cytokines over a period of at least 2 weeks, with the potential to increase past that point if required. It was hypothesized that being able to sustain this delivery and change the factor being delivered would significantly reduce the inflammatory reaction of macrophages and astrocytes, leading to a reduction in scar tissue formation and a probe that functions better long-term. Tests were performed on both macrophages as they form the initial response to an injury, and astrocytes as they also release inflammatory factors, and they make up 30–65% of glial cells in the brain and are the predominant cell within the glial scar.[1b] As both cells therefore play a significant role in immune reaction and scar formation, it was important to assess both reactions to sustained release of anti-inflammatory factors in order to strengthen any findings.[13] THP-1 monocytes, a human monocytic leukemia cell line, are used to form the macrophage model as these cells are widely used in inflammation studies. These cells have also been shown to exhibit similar inflammatory responses to microglia in vivo and blood-derived macrophages will also infiltrate upon probe insertion. In addition, the behavior of these macrophages correlates strongly with neuronal loss, a big concern for neuronal probe application.[14] For this study we chose not to look at the response of neurons themselves as this is often dependent on the glial response and it is difficult to maintain primary neurons chronically in vitro.[15] The response of neurons themselves will be assessed at the following in vivo stage in our future studies that have already been planned.

Furthermore, the dual-layered system designed to involve a drying stage to minimize the size and increase the stiffness of the implant for easy insertion in future clinical applications. It would also allow reswelling of the coating on insertion, which could reduce the damage to the surrounding tissue caused by micromotion of the electrode as well as making the electrode surface more mechanically compliant and similar to brain tissue. In order to ensure that the mechanical integrity of the microchannels was maintained during this cycle, and would be better sustained throughout implantation, reswelling tests were carried out and the effects of the addition of polyethylene glycol (PEG) to the gelatin methacryloyl (GelMA) layer to create a mechanically robust hydrogel was investigated. These hypotheses were tested by optimizing the design of the dual-layered coating in chip form and assessing the diffusion profile of differently sized molecules representing anti-inflammatory drugs through this dual-layered chip system. Once a final design was reached, the effect on macrophages and astrocytes of sustained release, from this dual-layered system, of dexamethasone (DEX) as an anti-inflammatory drug and interleukin-4 (IL-4) as an anti-inflammatory cytokine versus a single infusion of both factors over a 3-week period was investigated. The comparison versus single infusions through the dual-layered system was important to highlight that any additional improvements were coming from the system's ability to sustain delivery of the factors throughout the acute and into the chronic phase of immune response. In order to keep macrophages and astrocytes alive and representative of in vivo conditions, their surrounding environment was important, and therefore for both cells an optimization stage for their GelMA conditions was included to ensure the cells were initially in as a resting state as possible. As a proof of concept for future in vivo application, a thin dual-layered microfluidic device with hydrogel coating on the inner walls of the microchannel was fabricated and characterized for the diffusion profile of fluorescein isothiocyanate (FITC)-dextran.

2. Results and Discussion

2.1. Fabrication of Microchannel in Hydrogel

To fabricate a microchannel, we selected GelMA hydrogel that has been shown to support the growth of a wide variety of cells when the cells are either in contact with its surface or encapsulated within its structure.[16] It is also an enabling material for drug delivery applications as its porous structure can be fine-tuned to control the rate of drug release into the surrounding environment.[17] By optimizing the photocrosslinking time, mechanical properties of the hydrogel can also be exploited to easily fabricate and retain microchannels within the structure. However, particularly at lower concentrations, GelMA hydrogel can degrade quickly over time and diffusion through the hydrogel can be fast.[17b] For these reasons, as well as preventing excessive reswelling postinsertion and allowing even greater control over the drug release, a porous polydimethylsiloxane (PDMS) membrane layer was further added to the GelMA hydrogel containing the microchannel. PDMS is also nontoxic and nonbiodegradable[18] and the reduced surface area

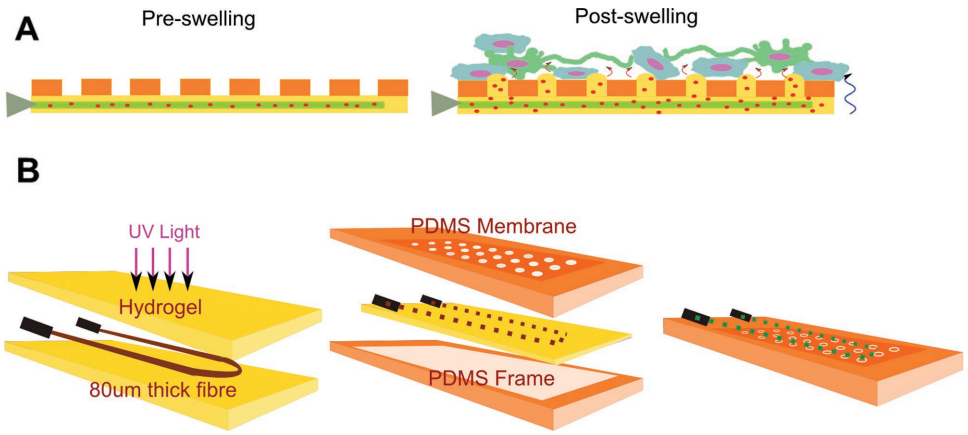

Figure 1. Construction of dual-layered microfluidic system and its concept. A) Schematic diagram illustrating the concept of the transformation from dry insertion state to drug delivering implantation state. B) Preparation procedure of microchannel in GelMA/PEG hydrogel construct surrounded by a microporous PDMS membrane.

for diffusion through the hydrogel-based microfluidic system could further slow the release of active molecules.

The concept and process for fabricating this system is illustrated in **Figure 1**. During the developmental process it was noticed that the drying and reswelling stages were having an adverse effect on the integrity of the hydrogel, particularly if they were left for more than 3 d in the dry state. The crosslinking of PEG and GelMA chains was to provide resistance to cracking upon drying by increasing the density of polymeric networks, resulting in improved mechanical strength of the composite hydrogel, similar to the result of composite hydrogel reported in our previous work.[19] The acryloyl substitution groups on the GelMA and PEG diacrylate (PEGDA) chains were covalently bonded after UV exposure resulting in a GelMA/PEG composite hydrogel. For this reason, three different hydrogel formulations were investigated: 5% GelMA, 10% GelMA, and 10% GelMA/2% PEG. First, their mechanical properties with varying degrees of photocrosslinking postdrying and reswelling were analyzed. The compressive moduli of 5% GelMA, 10% GelMA, and 10% GelMA/2% PEG hydrogel were 2.83 ± 0.40 kPa, 3.26 ± 0.45 kPa, and 6.41 ± 0.67 kPa, respectively (**Figure 2**A). As the compressive modulus of the brain tissue is around 1 kPa,[20] all of these formulations are strong enough to resist deformation by the brain tissue itself while not being so stiff that they cause a mechanical mismatch between the implant surface and the brain, which has been shown to increase the brain's immune reaction to implants.[21] The reswelling profiles of the three formulations were also assessed in order to ascertain if they would exert undue pressure on the brain and if their reswell time had the potential to be problematic in surgery, as implants have to be removed and reinserted several times during this time.[22] All three formulations had similar reswelling profiles with total reswell within 4 h in phosphate buffered saline (PBS, Figure 2B). The thicknesses of the hydrogels in their dry state were 210 ± 40 µm, 430 ± 20 µm, and 350 ± 20 µm, respectively. After 72 h of drying in air, the 10% GelMA/2% PEG hydrogel was the only formulation that remained entirely crack free among all samples. For this reason, as well as its thickness of only 350 ± 20 µm in the dry state, this formulation was chosen for fabrication of the device. Scanning electron microscopy images taken of this hydrogel (Figure 2C) show the porous structure of the hydrogel with pores of 90 ± 37 µm in diameter. The device itself was designed as a square piece with one single cylindrical microchannel of 80 ± 16 µm through the hydrogel in order to simplify verification of the diffusive gradient (Figure 2D). In practice however, the channel would be a loop to allow easier filling and emptying of the channel and this was also fabricated in order to show that this loop structure would be possible in the future. The appearance of the device itself as well as the microchannel and porous PDMS membrane under the microscope are shown in Figure 2E–H with the hydrogel stained green.

2.2. Diffusion through the Scaffold

To evaluate the diffusion of potential anti-inflammatory factors such as drug and interleukins through our system, FITC-dextran with various molecular weights (M_w) were used. DEX is a commonly used anti-inflammatory drug, particularly at the acute stage of inflammation and has a M_w of 392 Da.[15,23] FITC isomer has a M_w of 389 Da and has been used as a model for DEX. Interleukins are a family of cytokines involved in the inflammatory process and some of these such as IL-4 have been shown to have anti-inflammatory effects.[24] IL-4 has a M_w in the range of 12–20 kDa, and therefore FITC-dextran with 20 kDa was chosen as a model for this cytokine, with tests also conducted with 40 kDa FITC-dextran as a model for larger proteins that may be investigated at a later stage. In order to evaluate the diffusion of these FITC-based molecules, sample dual-layered microfluidic chips were placed under the fluorescent microscope and a single injection of the substance was added to the microchannel (**Figure 3**A(i)). The channel and its surrounding hydrogel area were imaged every 2 min until the dye had diffused throughout the chip (Figure 3B). The fluorescence intensity was significantly decreased by increasing the M_w of FITC variants and then decreased after saturation by diffusion of FITC variants through the hydrogel (Figure 3C).

The diffusion of the anti-inflammatory factors through the whole chip including the porous PDMS membrane and into

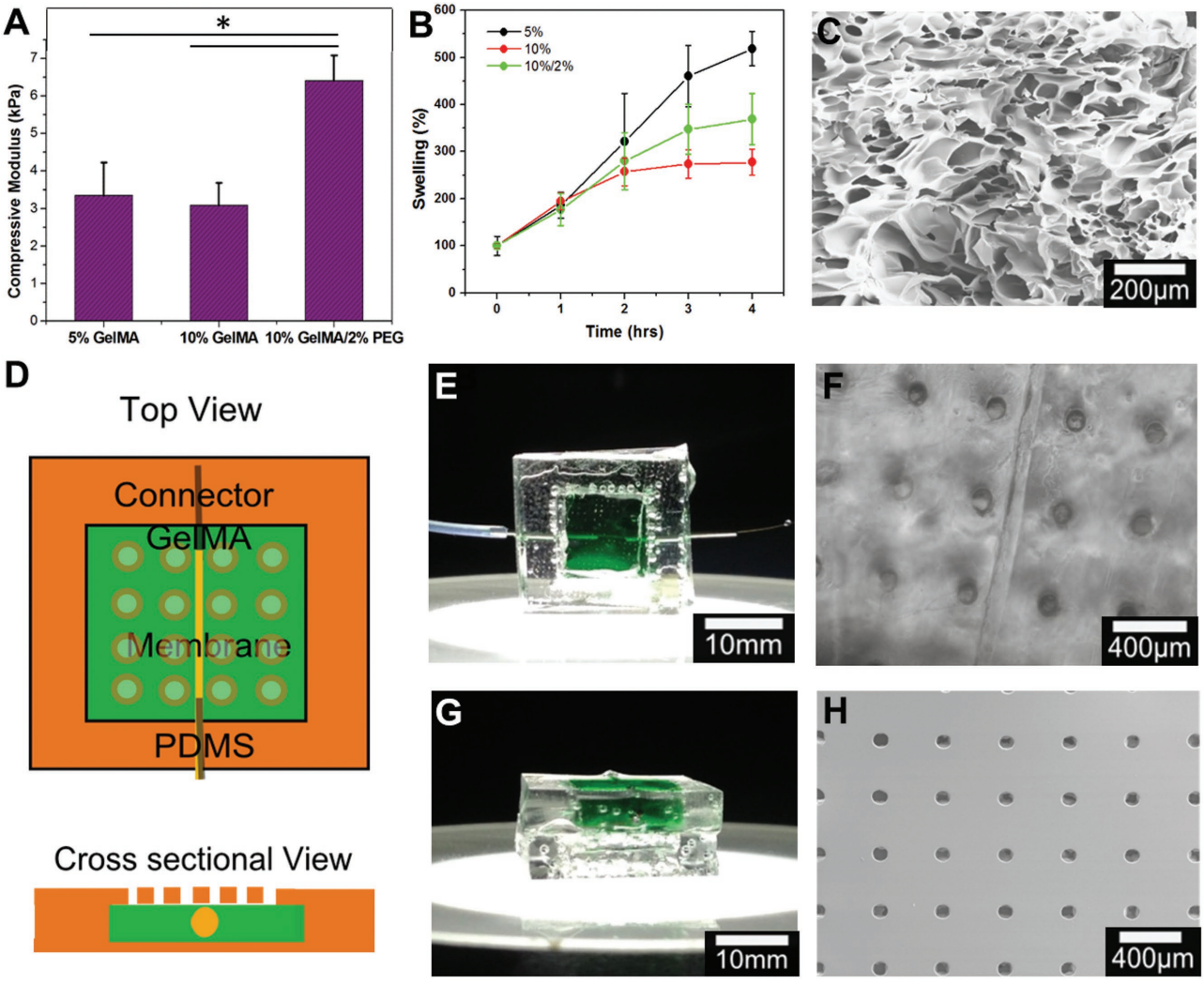

Figure 2. Chip design optimization. A) Compressive modulus of three different concentrations of GelMA/PEG hydrogel composites (*$p < 0.05$). B) Reswelling profiles of three different concentrations of GelMA/PEG hydrogel composites (*$p < 0.05$). C) Microstructure of GelMA/PEG composite hydrogel captured using scanning electron microscopy. D) Schematic of chip design. E) Top view of sample chip with GelMA/PEG composite hydrogel section stained green. F) Optical image of top view of chip showing 100-μm channel and 100-μm pores. G) Cross-sectional view of sample chip with GelMA/PEG section stained green. H) Scanning electron microscope image of PDMS membrane with 100-μm pores with 400-μm spacing.

the brain tissue on the other side is actually more relevant to our studies as this will allow us to specifically target different points in the inflammatory process with our molecules in future. This was evaluated by adding a PBS reservoir on top of the chip into which the FITC variants could diffuse over time (Figure 3A(ii)). Samples from this PBS reservoir could then be measured for fluorescence at regular intervals and the entire PBS reservoir replaced to maintain sink conditions as would be present in the brain. The obtained intensity of fluorescence signals were correlated to the concentrations of the FITC variants using the calibration curves of each FITC variants. Concentration of the FITC variants was plotted against time at 24 h intervals to identify peak release from the system and to assess the release profile (Figure 3D). The 40-kDa FITC-dextran had its peak release at 48 h while both 20- and 40-kDa FITC-dextran could be released from the system for up to 4 d after the initial infusion through the microchannel. This delayed peak release could be utilized when trying to release factors at precise stages of inflammatory reaction for an optimized drug delivery profile in future. As the release of FITC isomer and the 20-kDa FITC-dextran both peaked at 24 h or before, the experiment was repeated with 8 h time points (Figure 3E). This showed the initial release of the 20-kDa FITC-dextran was steady over the first 24 h and there was minimal burst release of the FITC isomer, a common problem with drug delivery systems.[10] These results showed an interesting contrast to the diffusion behavior of FITC variants through the hydrogel previously (Figure 3C), where the diffusions of the 20- and 40-kDa FITC-dextran were not significantly different. This may be due to the addition of the porous PDMS membrane that was further slowing down the diffusion of dextran into the PBS reservoir. These findings resulted in the decision to diffuse molecules twice a week for future chronic cell trials to ensure that cells would have a constant supply of our anti-inflammatory factors delivered to them.

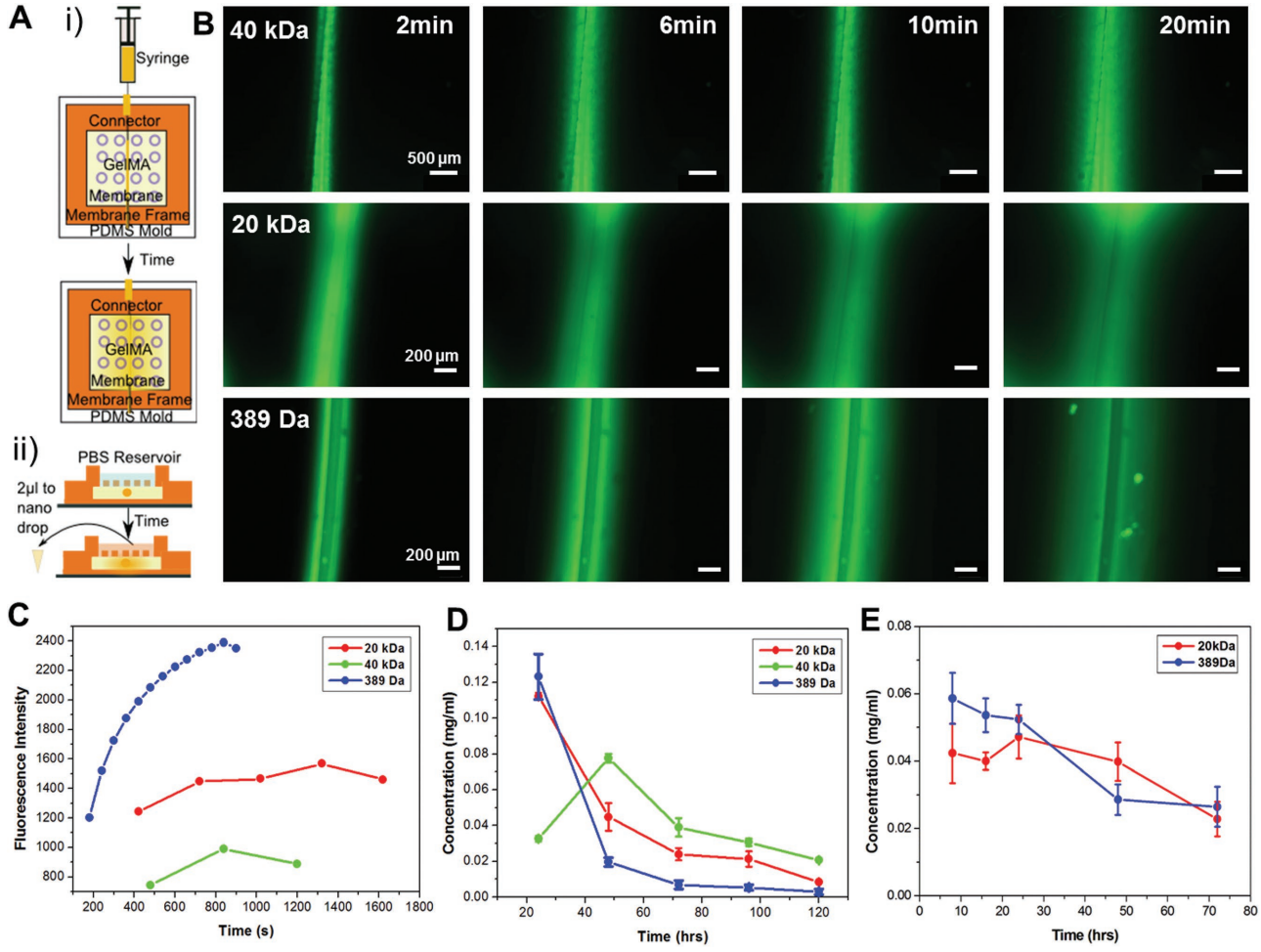

Figure 3. Diffusion profiles of FITC variants with different molecular weights through chip system. A) Schematic of tests to show diffusion: (i) optical set-up using microscope images and (ii) quantification using nanodrop to measure diffusion into a PBS reservoir. B) Fluorescence images over time of FITC-dextran (40-kDa M_w and 20-kDa M_w, respectively) and FITC isomer (389-Da M_w) showing effect of molecular weight on diffusion time. C) Progression of fluorescent signal at a point 100 µm away from microchannel as FITC diffuses through hydrogel system. D) Concentration of FITC isomer and FITC-dextran with different molecular weights diffused through the porous PDMS membrane into PBS reservoir at 24 h time points. E) Concentration of FITC isomer and FITC-dextran with different molecular weights diffused through the porous PDMS membrane into PBS reservoir at 8 h time points.

2.3. Monocyte Model Development and Chronic Drug Study

Once the drug delivery chip had been designed and optimized, a model of the brain was developed (**Figure 4**). As microglia are the first response to any injury in the brain, moderating their response can affect the whole chain of inflammation events.[13a] Microglia are sometimes referred to, as the macrophages of the brain as they carry out many of the same duties that macrophages carry out in the rest of the body.[25] Microglia are difficult to harvest and purify without having other remaining cell types, whereas macrophages can be formed from monocytes using a well-established cell line THP-1. As both macrophages and microglia have the ability to differentiate into M1 or M2 phenotypes, which correspond to pro-inflammatory and anti-inflammatory macrophages, respectively, monocytes represent a suitable model for investigating the effects of a drug delivery profile on the brain.[26] In order to create a more brain-like environment and allow longer survival of the cells, GelMA hydrogel was used as a 3D scaffold to imitate the brain-like extracellular matrix. The photocrosslinkable nature of this hydrogel allowed the fine-tuning of the mechanical properties to mimic brain tissue as a 20-s UV light exposure resulted in a compressive modulus of 1.27 ± 0.17 kPa, which is similar to brain tissue (Figure 4A).[20] Live/dead analysis of the encapsulated monocytes at these conditions was carried out at days 0 and 7 of encapsulation without drug delivery treatment (Figure 4B,C). The live cells are shown in green and the red indicates dead cells, indicating over 90% cells remaining viable at day 0 and over 80% at day 7.

Different test conditions for the drug delivery profile were designed and performed (Figure 4D). The profiles chosen consisted of a negative control with no infusions, an initial DEX infusion with subsequent twice per week DEX infusions, a single IL-4 infusion, an initial DEX infusion with subsequent twice per week IL-4 infusions, and an initial IL-4 infusion and subsequent twice per week IL-4 infusions (Table S1, Supporting Information). All infusions were injected directly into the dual-layered microfluidic chip, upon which a macrophage-laden

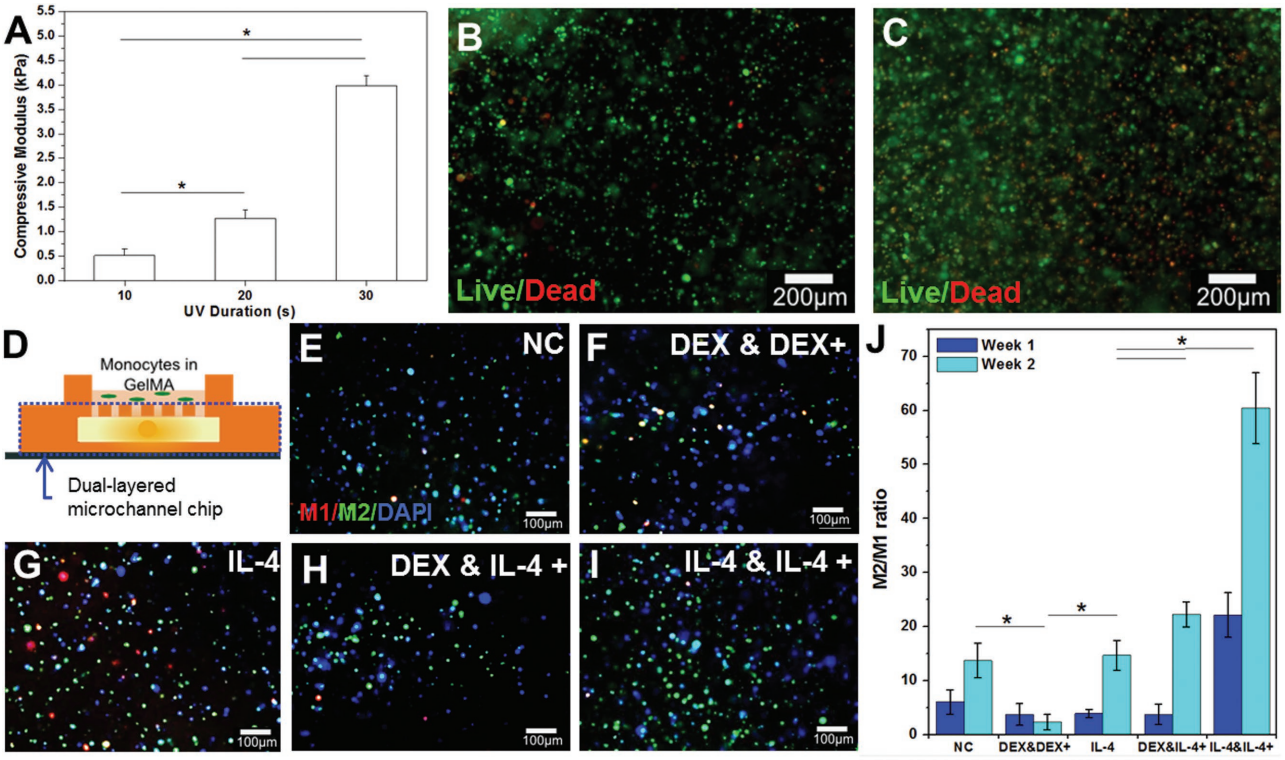

Figure 4. Phenotype of monocyte cells encapsulated in the 5% GelMA system as an in vitro model for brain immune response after different drug delivery profiles were delivered through the dual-layered microchannel chip system. A) Compressive modulus of monocytes encapsulated in 5% GelMA hydrogel with various UV time (*$p < 0.05$). Fluorescent images of monocytes stained using calcein (green) for live cells and ethidium homodimer-1 (red) for dead cells at B) day 0 and C) day 7. D) Schematic of experimental set-up showing monocytes encapsulated in GelMA hydrogel on top of the dual-layered microchannel chip. Immunostaining of CD206 (green) as an M2 macrophage, nuclei (blue), and 27E10 (red) as an M1 macrophage for samples with: E) no infusions (negative control); F) an initial DEX infusion and repeated DEX infusions; G) an initial IL-4 infusion only; H) an initial DEX infusion and repeated IL-4 infusions; I) an initial IL-4 infusion and repeated IL-4 infusions at week 1. J) Ratio of M2:M1 differentiated macrophages for all delivery profiles at 1 and 2 weeks indicating that repeated infusion of IL-4 significantly increases the presence of anti-inflammatory M2 macrophages (*$p < 0.05$).

hydrogel was placed in order to simulate delivery from a probe coating into the brain. When quantifying the ratio of cells with M2 (green) anti-inflammatory versus M1 (red) pro-inflammatory phenotypes, the negative control showed an increase from week 1 to week 2 without any infusion of anti-inflammatory factors, implying that the chips themselves do not have an adverse effect on the cells (Figure 4E–I,J). At week 2, the negative control statistically had the same ratio of M2:M1 cells as the samples with only one infusion of IL-4 and was performing better than those with repeated injections of DEX. Due to the use of a high concentration of DEX (0.1 mg mL^{-1}: $\approx 333 \times 10^{-9}$ M)[27] compared with previously reported studies that used 10×10^{-9} or 100×10^{-9} M DEX to induce M2 macrophage polarization,[28] it may have induced cytotoxicity during infusion of DEX to the monocyte model. By week 2 both conditions that involved repeated injections of IL-4 resulted in significantly increased ratios of M2:M1 macrophages, with the samples of IL-4 initial and IL-4 follow-up injections increasing the ratio sixfold compared with the negative control at the same time point (Figure 4J). This increase in M2 macrophages as a result of IL-4 stimulation was also observed for macrophages directly seeded onto IL-4-incorporated poly-L-lysine/hyaluronic composite films, along with a reduction in expression of inflammatory cytokines tumor necrosis factor (TNF)-α, IL-12, and IL-1β.[29] In order to strengthen these findings in the next stage we repeated the tests with primary astrocytes (the main cell type in a glial scar) and carried out immunoassays for released inflammatory cytokines.

2.4. Development of Brain-Like Tissue Model and Chronic Study for Astrocyte Model

3D astrocyte models are advantageous as, without a matrix to support their growth and network formation, the cells will die within a few days, and therefore chronic studies cannot be carried out.[30] These 3D models are also a more accurate representation of the brain structure. In order to form networks, astrocytes need a precise extracellular environment, and otherwise the cells would stay circular and die without behaving as astrocytes would in vivo.[30] For this reason, a variety of different percentages of photoinitiator (PI) and UV exposure time were tested in order to find the optimum parameters for healthy network formation. An initial screening immediately eliminated some combinations for being too weak to properly encapsulate cells and survive long term in an in vitro environment

(Table S2, Supporting Information). The promising combinations had cells encapsulated in 600-µm thick hydrogels, leaving cells to survive in vitro for a week for them to extend their processes and make connections with each other. These hydrogels were then imaged up to 200-µm deep into the structure so that a 3D representation of the cells could be built up. Neither 20-s UV/0.5% PI or 40-s UV/0.5% PI was suitable with very few cells having outgrowth and a lot of cell death apparent (Figure S1A,B, Supporting Information). 30-s UV/0.5% PI and 40-s UV/0.3% PI both showed some cell network formation but also many round dead cells (Figure S1C,D, Supporting Information). The optimum conditions for cell network formation were found to be the hydrogel with 0.3% PI and 30-s UV exposure as the majority of the cells had outgrowth with multiple connections and strong networks (Figure S1E, Supporting Information). The cross-section of the 3D image shows how this network spread throughout the entirety of the hydrogel and for this reason these conditions were chosen for the astrocyte model to test our drug delivery profiles (**Figure 5**A).

To test chronic drug delivery for the in vitro astrocyte model, we applied drugs with different delivery profiles (Table S3, Supporting Information) similar to the chronic study for the monocyte model. By the end of 3 weeks, both the negative control and the samples with DEX injections only had some astrocytes with long extended processes but no evidence of a strong network of cells (Figure 5B,C). The samples with a single injection of IL-4 showed an increased number of live cells with the formation of a more substantial network (Figure 5D). However, the samples with repeated IL-4 injections clearly had the healthiest networks of astrocyte cells (Figure 5E,F). ELISA immunoassays were also used to calculate the expression of inflammatory markers from the cell encapsulated hydrogels at week 1 and week 3. TNF-α is often viewed as the most consistent and unambiguous marker for cell inflammation,[31] and its release from samples was measured at week 1 and week 3 (Figure 5G). There was no significant difference between samples at 1 week and 3 weeks, indicating that inflammation is stable throughout this period. The negative control had significantly increased inflammation

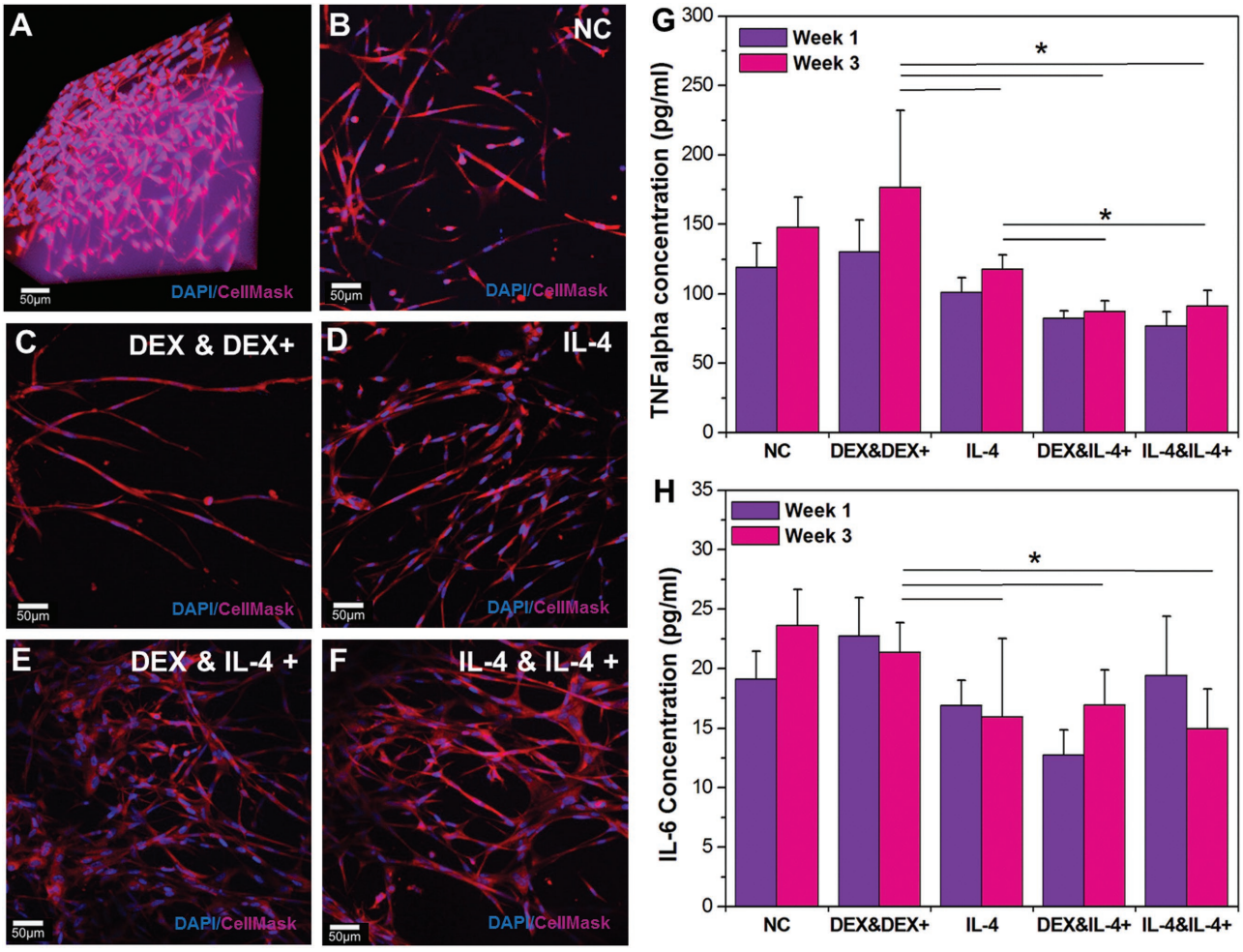

Figure 5. Confocal stacks images of hydrogel-encapsulated astrocytes after 3 weeks of different drug delivery profiles from the dual-layered microfluidic chip system. A) A 3D reconstruction image of optimized 3D astrocyte models with DAPI staining (blue) for nuclei and Cell Mask 649 (red) for cell structure at week 1. Chronic study samples with: B) no infusions (negative control); C) an initial DEX infusion and repeated DEX infusions; D) an initial IL-4 infusion only; E) an initial DEX infusion and repeated IL-4 infusions; F) an initial IL-4 infusion and repeated IL-4 infusions. G) Pro-inflammatory marker TNF-α release for each profile at weeks 1 and 3 (*$p < 0.05$). H) Pro-inflammatory marker IL-6 release for each profile at weeks 1 and 3 (*$p < 0.05$).

versus those with a single IL-4 injection, DEX and a repeated IL-4 injection, and IL-4 repeated injections only with *p*-values of 0.03, 0.0004, and 0.0002, respectively. Repeated DEX injections did not cause significant changes in inflammation versus the negative control or the IL-4 single injection; however, both DEX ($p = 0.02$ and $p = 0.03$) and IL-4 single injections ($p = 0.01$ and $p = 0.02$) had significantly higher amounts of TNF-α released than the repeated IL-4 injections. There was no significant difference in the repeated IL-4 injections between those injected with DEX or IL-4 initially, which implies that it is the repeated nature of IL-4 injections causing the reduction in inflammation over the 3-week period.

IL-6 is another marker of inflammation and its expression was also measured at 1 and 3 weeks (Figure 5H). There were no significant changes in inflammation between the negative control, the repeated DEX injections, or the IL-4 single injection. All samples with repeated IL-4 injections had significantly reduced release of IL-6 versus the negative control ($p = 0.01$ and 0.003) or the repeated DEX injected samples ($p = 0.04$ and $p = 0.002$). Interestingly, there was no significant difference between any of the repeated IL-4 injections or a single IL-4 injection, implying that the first few days of inflammation may be the most significant when it comes to releasing IL-6. Overall, both TNF-α and IL-6 release data show that repeated injections of IL-4 could be used to reduce the inflammatory response of the brain tissue to an electrode over time, although it must be noted that TNF-α expression did still slightly increase between weeks 1 and 3.

2.5. Development of Thin Dual-Layered Microfluidic System on the Metal Probe

To prove the possibility of the usage of the coating for delivery of anti-inflammatory molecules from a neural probe for future in vivo evaluation, we further developed a thin microfluidic device (thickness: ≈600-µm) containing a 10% GelMA/2% PEG composite hydrogel microchannel and integrated it to one side of a metal probe (450 µm in diameter) (**Figure 6**A). The microchannel with ≈5.5 cm in length, ≈150 µm in height, and ≈120 µm in width was fabricated using an SU-8 mold and then covered by a thin porous PDMS membrane with 200-µm pores and 100-µm thickness. The fabricated thin microchannel was easily bonded to one side of the metal probe using additional PDMS, leading to a total thickness of whole construct of ≈1.5 mm similar to that of current DBS electrodes in the market and therefore a clinically viable option (Figure 6A). Although some research shows that decreasing the size of electrodes reduces the inflammatory response,[32] alternative studies indicate that although the acute response is reduced, this often is not witnessed in long term.[11a] However, mechanical injury should be assessed in vivo at a later stage.

To create the hydrogel layer, 10% GelMA/2% PEG prepolymer solution was flown through the microchannel while being exposed to UV light for crosslinking GelMA and PEG. GelMA/PEG composite hydrogel was uniformly coated on the inner wall of the microchannel with ≈30-µm thickness as shown in Figure 6B. The thickness of the GelMA/PEG coating in the microchannel however, could potentially be controlled by flow rate and concentration of the prepolymer solution and UV exposure time.[33] To confirm the diffusion of anti-inflammatory drugs through the GelMA hydrogel coating and the porous PDMS membrane in the thin microfluidic device, FITC-dextran with 20-kDa M_w was perfused through the microchannel and imaged at various intervals (Figure 6C). Fluorescence intensity quantified at a point 30-µm from the middle of the channel displayed the profile of the formation of the FITC-dextran gradient and the average distance FITC-dextran diffused (Figure 6D,E). In addition, the rate of diffusion via the thin microfluidic device could be controlled by changing the composition of the coating hydrogel. The thin microfluidic device coated by the 14% GelMA hydrogel showed faster diffusion of FITC-dextran with 20-kDa M_w than that of GelMA/PEG-coated device (Figure S3, Supporting Information). It was clear that this microfluidic setup provided a uniform diffusion profile through the GelMA/PEG coating and the porous PDMS membrane, indicating its potential translation for in vivo applications in the future.

3. Conclusions

A dual-layered microfluidic system was developed for use as a coating for neural electrodes which could be inserted in a thin dry state and then be held firmly in place by its own reswelling, protecting the brain against damage caused by micromotion of the electrode. The system can easily be infused with a range of anti-inflammatory factors at body temperature for a period of at least 3 weeks without degradation and this profile of infusion has the potential to be fine-tuned to target specific phases of the brain's immune reaction. The system allows the steady release of cytokines for at least 4 days from one infusion and has a minimal burst release of small molecules. In order to assess the potential anti-inflammatory effects of factors delivered through the designed dual-layered microfluidic system, a number of glial cell models were developed and optimized, before using the chip to deliver factors and measure their effect upon the cells. Therefore, two different hydrogels with optimized cell-specific mechanical properties encapsulated with either monocytes or astrocytes were developed as brain-like models and these hydrogels were able to last in an in vivo-mimicking environment for a minimum of 2 and 3 weeks, respectively. The repeated infusion of IL-4 caused both an upregulation in M2-induced macrophages over 2 weeks and a downregulation of both TNF-α and IL-6 in astrocytes over a 3-week period. Further work could involve the development of an encapsulated coculture of microglia and astrocytes as a more realistic model for the brain in vitro. DEX infusion had no effect on either of these measured outputs; however, further work must be done to assess the mechanisms and the anti-inflammatory effects of DEX as these are well recognized elsewhere in the body. These improvements in anti-inflammatory effects in vitro imply that repeated infusions of anti-inflammatory factors like IL-4 could be utilized in the future to reduce the formation of a glial scar around neural implants and increase their efficacy long-term. A thin dual-layered microfluidic device with GelMA/PEG coating on the inner walls of the microchannel and a porous PDMS membrane, wrapped on a metal probe, was also fabricated for the proof of concept demonstration of the

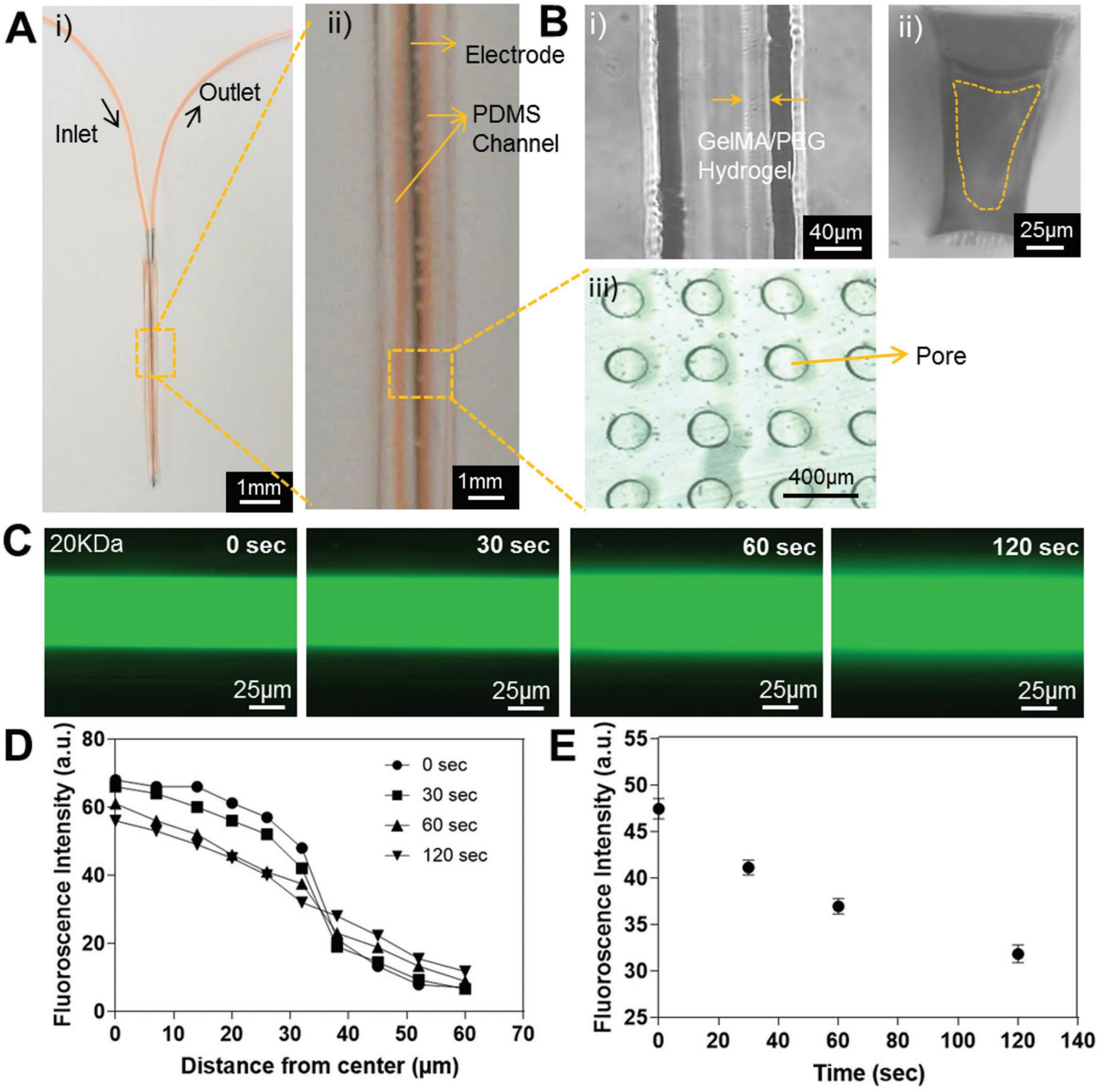

Figure 6. A) The thin dual-layered microfluidic device integrated on a metal probe. (i) Top view and (ii) magnified top view with microchannel in orange color. B) Brightfield image of the GelMA/PEG hydrogel coating inside the microchannel. (i) Top view; (ii) cross-sectional view; and (iii) porous PDMS membrane. C) Fluorescence images showing the diffusion of FITC-dextran (20-kDa M_w) at different time points. D) Quantification of fluorescence intensities measured from the middle to the side along its radius of the microchannel at different time points. E) Time-lapse fluorescent signal change at a point 30 μm from the middle of the microchannel.

delivery of anti-inflammatory molecules through GelMA/PEG coating from a neural probe. This thin microfluidic system can be coated onto or be embedded in neural probes for in situ delivery of multiple anti-inflammatory factors for future in vivo evaluations, with a focus on the cellular and vascular structures at the probe–tissue interface for periods of time of 3 weeks and greater. The system may also find other potential drug delivery applications in the wider implant and medical device industry that are being explored.

4. Experimental Section

Synthesis of GelMA: Gelatin from porcine skin (Sigma-Aldrich) was dissolved at 10% (w/v) in 100 mL PBS at 50 °C for 1 h.[34] Next, 8 mL methacrylic anhydride (Sigma-Aldrich) was slowly added to the gelatin solution and stirred at 50 °C for 2 h before an additional 100 mL of PBS was added and mixed at 50 °C in order to stop the reaction. The obtained solution was dialyzed at 40 °C for 7 d using dialysis membranes (M_w cut off: 12–14 kDa, Fisher Scientific). The purified solution was filtered using a vacuum filtration cup with 0.22-μm pores (Millipore). This solution was frozen to –80 °C before freeze drying for 5 d.

GelMA Solutions: Prepolymer solutions of 5% GelMA for cell encapsulation were prepared with 0.5% PI (2-hydroxy-1-(4-(hydroxyethoxy) phenyl)-2-methyl-1-propanone 98%, Sigma-Aldrich) in PBS. For scaffold manufacturing, 10% GelMA, 2% PEGDA (1000 M_w, Polysciences), and 0.5% PI solutions were used. All UV crosslinking was carried out at 6.9 mW cm^{-2}.

Fabrication of PDMS Membranes: All PDMS was prepared at a ratio of 10:1 with its curing agent (Sylgard 184 Silicone Elastomer Kit, Dow Corning). PDMS membranes of 100-µm thick were fabricated using a silicon wafer with 100-µm diameter posts spaced 400 µm apart. The thin PDMS membrane was formed using a spin coater at 3500 rpm for 2 min before scraping over the posts with a glass slide. Partially cured PDMS frames of 0.5 cm (width) × 0.5 cm (length) (cured for 20 min in an 80 °C oven) were added on top of the fresh PDMS on the mold before curing at 80 °C for 2.5 h to produce membranes with attached frames.

Fabrication of Microchannel in Hydrogel: To create microchannel in GelMA/PEG composite hydrogel, molds of 0.25 cm^2 were manufactured from PDMS as described previously.[35] Small metal connectors (100-µm inner diameter) were punched through the middle of the mold and a sacrificial fiber of 80 µm thickness was passed through the connectors. The mold was filled with 80 µL of 10% GelMA/2% PEG solution before UV crosslinking for 60 s. These samples were air-dried for 12 h. The PDMS membrane and frame was then plasma-bonded on top and PBS was added to allow reswelling of the construct for a number of hours. At this stage the sacrificial fiber was removed to create a microchannel of 80 µm diameter through the center of the construct (Figure 1).

Fabrication of Hydrogel-Coated Thin Microfluidic Device: The device had two parallel and connected channels of 5.5 cm long, 120 µm wide, and 150 µm high. The devices were fabricated using standard photo- and soft-lithography protocols. Briefly, a master silicon wafer (Silicon Sense, Inc.) was patterned with negative photoresist (SU8-2100, MicroChem Corp.) by spin-coating at 1850 rpm for 40 s, followed by a soft bake (5 min at 65 °C and 22 min at 95 °C) and UV exposure at 260 mJ cm^{-2}. These resin-coated wafers were postexposure baked (5 min at 65 °C and 10 min at 95 °C) and developed using propyleneglycol methyl ether acetate (484431, Sigma-Aldrich), followed by a 30-min long hardening bake at 180 °C. The microfluidic channels were subsequently generated in 500-µm thick PDMS (Sylgard 184, Dow Corning) by spin-coating and further sealed with a porous PDMS membrane described in the section "Fabrication of PDMS Membranes" of the Experimental Section using oxygen plasma. To successfully bond the thin microfluidic device, the metal probe was coated by a thin layer of PDMS with 200 µm in thickness. Thin microfluidic device was then bonded on the PDMS-coated metal probe by oxygen plasma treatment. To connect the microchannel in the device, metal connectors and tygon tubes were used. A 10% GelMA and 2% PEG solution containing 0.5 wt/vol% PI in PBS was introduced into the microchannel by a syringe pump at a flow rate 2 mL h^{-1} and was crosslinked under UV light for 3 min at 14.6 mW cm^{-2} (Figure S2, Supporting Information). The uncrosslinked GelMA/PEG prepolymer solution was washed with PBS for 4 min. The entire PDMS structure was sandwiched between two glass plates before exposing to the UV light. The GelMA/PEG-coated devices were stored in PBS for diffusion studies. Using same method, the thin microfluidic device was coated by 14% GelMA solution containing 0.8 wt/vol% PI in PBS.

Diffusion Studies: For thick microfluidic chip, diffusion was tested optically using FITC-dextran with 20-kDa M_w as a model for IL-4 (M_w: 12–20 kDa), 40-kDa M_w as a model for larger proteins, and 389-Da M_w FITC isomer as a model for DEX (Sigma-Aldrich). A solution of 20 mg mL^{-1} of FITC-dextran in PBS was injected into the microchannel until it was full and fluorescent images were taken from above every 5 min at 37 °C. A 100 µL reservoir of PBS was added to the top of the PDMS membrane and stored in a humidified chamber in an incubator at 37 °C. Every 24 h the 100-µL was replaced in order to maintain sink conditions and the fluorescence of 2 µL of the solution was measured using Nanodrop2000 (Thermo Fisher Scientific). Blank measurements were conducted using PBS and all measurements were completed using triplicates of 2 µL samples. FITC-dextran was measured at 494 nm excitation levels and concentrations were calculated using a calibration curve. For the thin microfluidic device on the metal probe, diffusion through the GelMA coating was evaluated using FITC-dextran with a 20-kDa M_w. A solution of FITC-dextran of 12 mg mL^{-1} in PBS was injected inside the microchannel and the images were taken at 0, 30, 60, and 120 s. The fluorescent images were processed using imageJ and the fluorescent intensities across different sections of the channel and different time points were calculated.

Microscope Imaging: All bright field and fluorescent images were taken on a Zeiss Axio Observer D1 Fluorescence Microscope (Carl Zeiss, Germany) and all scanning electron microscopy images were taken on a Hitachi Model S4700, Japan. Confocal images were taken on Leica SP5X MP, Germany.

Mechanical Properties of Hydrogel: Mechanical properties of the hydrogels were calculated using Instron 5524 mechanical analyzer (Instron, Canton, MA) compressive tests with a 10 N load cell. Compressive modulus was calculated between 10 and 20% loading of 600-µm thick samples with a 5-mm diameter with 6 replicates for each sample.

Monocyte Culture and Encapsulation: THP-1 monocyte cells (ATCC) were cultured in suspension for at least 7 d before use in Roswell Park Memorial Institute Medium (RPMI) (Life Technologies) supplemented with 10% fetal bovine serum (FBS) (Gibco BRL) and 1% Penicillin-Streptomycin (Gibco BRL) at 0.5–2 million cells mL^{-1} media. Cell media was changed every three days, retaining 20% of the old media. Monocytes were encapsulated in 5% GelMA hydrogel with 6 million cells mL^{-1} and 50 µL of this solution was added on top of the chip and UV crosslinked as before for 20 s.

Astrocyte Culture and Encapsulation: Primary human astrocytes (ScienceCell) were cultured from suspension at least 7 d before use in media (Dulbecco's modified eagle medium (DMEM):F12 with L-glutamine + 4-(2-hydroxyethyl)-1-piperazineethanesulfonic acid (HEPES), Thermoscientific) supplemented with 10% FBS (Sigma-Aldrich), 10% Astrocyte Growth Supplement (ScienceCell), and 1% Penicillin-Streptomycin (Sigma-Aldrich) at 0.5–2 million cells mL^{-1} media. Cell media was changed at least every three days, retaining 50% of the old media. Astrocytes were encapsulated in 5% GelMA hydrogel with between 0.1 and 0.5% PI at a density of 1 million cells mL^{-1} whereby 50 µL of solution was added to the top of the chip and subjected to between 20 and 40 s of UV light exposure.

Chronic Cell Studies: Each sample had an initial infusion of 0.1 mg mL^{-1} DEX (Sigma-Aldrich) or 10 ng mL^{-1} IL-4 (R&D Systems) through the microchannel, excluding negative controls. Selected samples then had repeated infusions (every 3.5 d) of IL-4 or DEX (Table S1 and S3), with media added every 3.5 d immediately before injections. Immunostaining was carried out at days 21.

Live/Dead Assay: Cell viability assays were carried out at days 1 and 7 using Live/Dead kits for mammalian cells (Life Technologies). After washing all samples in warm PBS, a mixed solution of ethidium homodimer-1 and calcein was prepared in a ratio of 4:1 and 300 µL of this solution was incubated for 15 min. After this period, samples were washed in PBS five more times, before being left in PBS for microscope imaging.

Immunostaining: All cell encapsulated hydrogel samples were washed with PBS before fixation in 4% paraformaldehyde (Sigma-Aldrich) at room temperature for 30 min. Samples were stored overnight at 4 °C in PBS at this stage if required. Samples were then incubated in 0.1% Triton x-100 (Sigma-Aldrich) at room temperature for 30 min. Blocking was carried out in 1% bovine serum albumin (BSA) (Sigma-Aldrich) in PBS at room temperature for 1 h. For monocyte samples, the primary antibody for CD206 as an M2 macrophage (R&D Systems) was diluted at 1:100 in PBS with 1% BSA and samples were incubated overnight at 4 °C in a humidified chamber. The Alexa 488 or Alexa 594 conjugated secondary antibodies (Molecular Probes) were added at a dilution of 1:200 in PBS with 1% BSA and incubated for 1 h at room temperature in a dark humidified chamber. The primary and secondary antibody addition steps were repeated for 27E10 as an M1 macrophage (R&D Systems) before adding 4,6-diamidino-2-phenylindole (DAPI, Vector Laboratories

Inc.) at 1:1000 dilution for 10 min at room temperature whereby samples were ready for observation under the microscope. Between each stage 3 × 5 min washes in PBS were carried out. For astrocyte samples, DAPI was added at 1:2500 dilution as well as Cellmask 647 membrane stain (Sigma-Aldrich) at 1:1000 dilution in a PBS 10% goat serum (Gibco BRL) solution at room temperature for 10 min after which samples were ready for observation under the microscope. Between each stage 3 × 5 min washes in PBS were carried out.

ELISA Assays: TNF-α and IL-6 sandwich ELISAs (R&D systems) were carried out according to supplier's instructions. Briefly, 50 µL of assay diluent and 200 µL of sample were added to each well for 2 h. Following four washes with the wash buffer, 200 µL of either TNF-α or IL-6 conjugate was added and left for a further 2 h period. After another wash cycle, 200 µL of the substrate solution was added and left for 20 min before the addition of a stop solution and the assay was measured at 450 and 540 nm using the plate reader.

Statistical Analysis: All data are expressed as mean ± standard deviation. *T*-tests or 2-way ANOVA tests were performed when appropriate with $^*P < 0.05$ being viewed as significant.

Supporting Information

Supporting Information is available from the Wiley Online Library or from the author.

Acknowledgements

L.F. and P.B. contributed equally to this work. This paper was supported by the Institute for Soldier Nanotechnology, National Institutes of Health (HL092836, EB012597, AR057837, HL099073), the National Science Foundation (DMR0847287), ONR PECASE, and the Higher Education Authority Ireland. S.R.S. would like to recognize and thank Brigham and Women's Hospital President Betsy Nabel, MD, and the Reny family, for the Stepping Strong Innovator Award through their generous funding. Many thanks to Fulbright Ireland Association for further funding and facilitating this collaboration between Trinity and Harvard-MIT Health Sciences.

Conflict of Interest

The authors declare no conflict of interest.

Keywords

astrocytes, drug delivery, hydrogels, microfluidic system, neural electrodes, neural probes

Received: April 15, 2017
Revised: June 26, 2017
Published online:

[1] a) S. P. Massia, M. M. Holecko, G. R. Ehteshami, *J. Biomed. Mater. Res., Part A* **2004**, *68*, 177; b) V. S. Polikov, P. A. Tresco, W. M. Reichert, *J. Neurosci. Methods* **2005**, *148*, 1; c) K. Udupa, R. Chen, *Prog. Neurobiol.* **2015**, *133*, 27.

[2] a) R. V. Bellamkonda, S. B. Pai, P. Renaud, *MRS Bull.* **2012**, *37*, 557; b) W. He, G. C. McConnell, T. M. Schneider, R. V. Bellamkonda, *Adv. Mater.* **2007**, *19*, 3529.

[3] a) Y. Lu, D. Wang, T. Li, X. Zhao, Y. Cao, H. Yang, Y. Y. Duan, *Biomaterials* **2009**, *30*, 4143; b) Z. Yue, S. E. Moulton, M. Cook, S. O'Leary, G. G. Wallace, *Adv. Drug Delivery Rev.* **2013**, *65*, 559; c) L. Rao, H. Zhou, T. Li, C. Li, Y. Y. Duan, *Acta Biomater.* **2012**, *8*, 2233.

[4] a) S. Pieperhoff, *Front. Physiol.* **2012**, *3*, 1; b) W. He, R. V. Bellamkonda, *Biomaterials* **2005**, *26*, 2983; c) G. K. Bergey, *Exp. Neurol.* **2013**, *244*, 87.

[5] L. R. Hochberg, D. Bacher, B. Jarosiewicz, N. Y. Masse, J. D. Simeral, J. Vogel, S. Haddadin, J. Liu, S. S. Cash, P. van der Smagt, J. P. Donoghue, *Nature* **2012**, *485*, 372.

[6] a) R. A. Green, N. H. Lovell, G. G. Wallace, L. A. Poole-Warren, *Biomaterials* **2008**, *29*, 3393; b) L. L. Jiang, J. L. Liu, X. L. Fu, W. B. Xian, J. Gu, Y. M. Liu, J. Ye, J. Chen, H. Qian, S. H. Xu, Z. Pei, L. Chen, *Chin. Med. J.* **2015**, *128*, 2433.

[7] C. S. Bjornsson, S. J. Oh, Y. A. Al-Kofahi, Y. J. Lim, K. L. Smith, J. N. Turner, S. De, B. Roysam, W. Shain, S. J. Kim, *J. Neural. Eng.* **2006**, *3*, 196.

[8] a) D. H. Szarowski, M. D. Andersen, S. Retterer, A. J. Spence, M. Isaacson, H. G. Craighead, J. N. Turner, W. Shain, *Brain Res.* **2003**, *983*, 23; b) R. Biran, D. C. Martin, P. A. Tresco, *J. Biomed. Mater. Res., Part A* **2007**, *82*, 169.

[9] a) D. B. McCreery, W. F. Agnew, T. G. Yuen, L. Bullara, *IEEE Trans. Biomed. Eng.* **1990**, *37*, 996; b) H. Liu, L. Zhu, S. Sheng, L. Sun, H. Zhou, H. Tang, T. Qiu, *J. Neural. Eng.* **2013**, *10*, 036024.

[10] K. A. Potter, M. Jorfi, K. T. Householder, E. J. Foster, C. Weder, J. R. Capadona, *Acta Biomater.* **2014**, *10*, 2209.

[11] a) D. H. Szarowski, M. D. Andersen, S. Retterer, A. J. Spence, M. Isaacson, H. G. Craighead, J. N. Turner, W. Shain, *Brain Res.* **2003**, *983*, 23; b) K. A. Potter, M. Jorfi, K. T. Householder, E. J. Foster, C. Weder, J. R. Capadona, *Acta Biomater.* **2014**, *10*, 2209.

[12] J. N. Turner, W. Shain, D. H. Szarowski, M. Andersen, S. Martins, M. Isaacson, H. Craighead, *Exp. Neurol.* **1999**, *156*, 33.

[13] a) W. Liu, Y. Tang, J. Feng, *Life Sci.* **2011**, *89*, 141; b) R. Yamasaki, H. Lu, O. Butovsky, N. Ohno, A. M. Rietsch, R. Cialic, P. M. Wu, C. E. Doykan, J. Lin, A. C. Cotleur, G. Kidd, M. M. Zorlu, N. Sun, W. Hu, L. Liu, J. C. Lee, S. E. Taylor, L. Uehlein, D. Dixon, J. Gu, C. M. Floruta, M. Zhu, I. F. Charo, H. L. Weiner, R. M. Ransohoff, *J. Exp. Med.* **2014**, *211*, 1533.

[14] a) M. Ravikumar, S. Sunil, J. Black, D. S. Barkauskas, A. Y. Haung, R. H. Miller, S. M. Selkirk, J. R. Capadona, *Biomaterials* **2014**, *35*, 8049; b) J. D. Cherry, J. A. Olschowka, M. K. O'Banion, *J. Neuroinflammation* **2014**, *11*, 98; c) R. Franco, D. Fernandez-Suarez, *Prog. Neurobiol.* **2015**, *131*, 65.

[15] Y. Zhong, R. V. Bellamkonda, *Brain Res.* **2007**, *1148*, 15.

[16] J. W. Nichol, S. T. Koshy, H. Bae, C. M. Hwang, S. Yamanlar, A. Khademhosseini, *Biomaterials* **2010**, *31*, 5536.

[17] a) K. Yue, G. Trujillo-de Santiago, M. M. Alvarez, A. Tamayol, N. Annabi, A. Khademhosseini, *Biomaterials* **2015**, *73*, 254; b) P. Coimbra, M. H. Gil, M. Figueiredo, *Int. J. Biol. Macromol.* **2014**, *70*, 10.

[18] a) A. Simmons, A. D. Padsalgikar, L. M. Ferris, L. A. Poole-Warren, *Biomaterials* **2008**, *29*, 2987; b) A. Agarwal, J. A. Goss, A. Cho, M. L. McCain, K. K. Parker, *Lab Chip* **2013**, *13*, 3599.

[19] C. B. Hutson, J. W. Nichol, H. Aubin, H. Bae, S. Yamanlar, S. Al-Haque, S. T. Koshy, A. Khademhosseini, *Tissue Eng., Part A* **2011**, *17*, 1713.

[20] S. Budday, R. Nay, R. de Rooij, P. Steinmann, T. Wyrobek, T. C. Ovaert, E. Kuhl, *J. Mech. Behav. Biomed. Mater.* **2015**, *46*, 318.

[21] S.-H. Huang, S.-P. Lin, J.-J. J. Chen, *Sens. Actuators, A* **2014**, *216*, 257.

[22] C. Joint, D. Nandi, S. Parkin, R. Gregory, T. Aziz, *Mov. Disord.* **2002**, *17*, Suppl 3, S175.

[23] a) D.-H. Kim, D. C. Martin, *Biomaterials* **2006**, *27*, 3031; b) L. Spataro, J. Dilgen, S. Retterer, A. J. Spence, M. Isaacson, J. N. Turner, W. Shain, *Exp. Neurol.* **2005**, *194*, 289.

[24] a) A. Michelucci, T. Heurtaux, L. Grandbarbe, E. Morga, P. Heuschling, *J. Neuroimmunol.* **2009**, *210*, 3; b) F. Y. McWhorter, T. Wang, P. Nguyen, T. Chung, W. F. Liu, *Proc. Natl. Acad. Sci. USA* **2013**, *110*, 17253.
[25] S. Losciuto, G. Dorban, S. Gabel, A. Gustin, C. Hoenen, L. Grandbarbe, P. Heuschling, T. Heurtaux, *J. Neurosci. Methods* **2012**, *207*, 59.
[26] a) D. M. Wilcock, *Int. J. Alzheimer's Dis.* **2012**, *2012*, 495243; b) E. Polazzi, B. Monti, *Prog. Neurobiol.* **2010**, *92*, 293; c) A. J. Sawyer, W. Tian, J. K. Saucier-Sawyer, P. J. Rizk, W. M. Saltzman, R. V. Bellamkonda, T. R. Kyriakides, *Biomaterials* **2014**, *35*, 6698.
[27] C. Ito, W. E. Evans, L. McNinch, E. Coustan-Smith, H. Mahmoud, C. H. Pui, D. Campana, *J. Clin. Oncol.* **1996**, *14*, 2370.
[28] S. Tedesco, C. Bolego, A. Toniolo, A. Nassi, G. P. Fadini, M. Locati, A. Cignarella, *Immunobiology* **2015**, *220*, 545.
[29] H. Knopf-Marques, S. Singh, S. S. Htwe, L. Wolfova, R. Buffa, J. Bacharouche, G. Francius, J. C. Voegel, P. Schaaf, A. M. Ghaemmaghami, N. E. Vrana, P. Lavalle, *Biomacromolecules* **2016**, *17*, 2189.
[30] A. L. Placone, P. M. McGuiggan, D. E. Bergles, H. Guerrero-Cazares, A. Quinones-Hinojosa, P. C. Searson, *Biomaterials* **2015**, *42*, 134.
[31] K. A. Frankola, N. H. Greig, W. Luo, D. Tweedie, *CNS Neurol. Disord.: Drug Targets* **2011**, *10*, 391.
[32] L. Karumbaiah, T. Saxena, D. Carlson, K. Patil, R. Patkar, E. A. Gaupp, M. Betancur, G. B. Stanley, L. Carin, R. V. Bellamkonda, *Biomaterials* **2013**, *34*, 8061.
[33] N. Annabi, S. Selimovic, J. P. Acevedo Cox, J. Ribas, M. Afshar Bakooshli, D. Heintze, A. S. Weiss, D. Cropek, A. Khademhosseini, *Lab Chip* **2013**, *13*, 3569.
[34] A. I. Van Den Bulcke, B. Bogdanov, N. De Rooze, E. H. Schacht, M. Cornelissen, H. Berghmans, *Biomacromolecules* **2000**, *1*, 31.
[35] N. Annabi, S. R. Shin, A. Tamayol, M. Miscuglio, M. A. Bakooshli, A. Assmann, P. Mostafalu, J. Y. Sun, S. Mithieux, L. Cheung, X. S. Tang, A. S. Weiss, A. Khademhosseini, *Adv. Mater.* **2016**, *28*, 40.